Chapter 11

Local Packing in Molecular Materials

Chapter Outline

11.1. INTRODUCTION

Although PDFs have been applied widely to study inorganic materials, including liquids, amorphous and, the main topic of this book, crystalline and nanocrystalline materials, much less attention has been placed on studying molecular materials. The study of the structure of molecules themselves has been widely done since the middle of the twentieth century using gas-phase electron diffraction, with analysis carried out using the Debye equation or the PDF (Mark and Wierl, 1930). There continue to be a number of active groups in the world with this specialized type of equipment (Belyakov *et al*., 2012; Shainyan *et al*., 2012; Spirk *et al*., 2012). As we discussed in Chapter 2, the next step for this research is to study excited-state structures by photoexciting the molecules with a laser and studying the structure using ultrafast electron diffraction, where the electron probe beam arrives some femto or picoseconds after the excitation laser pulse (Zewail, 2006).

Although it is important to know the structure of small molecules, it is often of equal importance to understand the molecular packing in the solid state. The properties of molecular solids depend sensitively on the packing arrangement. For example, different polymorphs (crystal structures) of molecular pigment molecules have different colors because of the differing molecular orbital overlaps that modify the electron levels giving rise to the color

Pergamon Materials Series, Vol. 16. http://dx.doi.org/10.1016/B978-0-08-097133-9.00011-3
© 2012 Elsevier Ltd. All rights reserved.

(Paulus *et al*., 2007). It is extremely important to control polymorphism in the pigment industry and for pigment structures to be stable over time in sometimes quite harsh conditions. Similar issues are of great importance in the world of molecular electronics, where the packing of molecules affects electronic transport a great deal (Kline *et al*., 2006).

The same is also true in the world of pharmaceuticals (Hancock and Zograf, 1997). Most pharmaceuticals are small molecules that dissolve and get into the blood stream of the patient. Typically, they find their way to infected cells and bind to proteins that play some crucial role in the life cycle of the disease, inhibiting the protein and disrupting the disease. Clearly, the molecular structure is important so that it binds and inhibits the right protein (and does not bind to the wrong proteins). However, it is difficult to see how the packing of the molecules is of any great importance. However, it turns out that, for drug delivery, the molecular packing is of the utmost importance. Things like the solubility and the solvation rate of the molecule in the stomach, and thus the bioavailability of the drug in pill form, depend sensitively on the molecular packing (Hancock and Parks, 2000). The former determines the dose of the drug and the latter the dose profile, which is the concentration of the drug in the blood stream as a function of time. Too little of the drug is not pharmacologically active and too much may be toxic. Thus, for reasons of safety and efficacy, drugs are approved for use, by agencies such as the Food and Drug Administration in the United States, in a particular crystalline form or polymorph. Another polymorph may also be acceptable if it can be shown to be safe and effective, and thus the discovery of the same drug in different crystalline forms takes on importance from an intellectual property perspective since the same drug may be patented more than once in different forms. Polymorph screening (i.e., searching for all the possible polymorphs and assessing their properties) is therefore a large part of the drug development process.

11.2. FINGERPRINTING

X-ray diffraction plays a big role in this since different polymorphs of the same drug have very different powder X-ray diffraction patterns (Bernstein, 2002). These patterns are used to "fingerprint" the different polymorphs. A pill made up of a powdered form of the drug, the active pharmaceutical ingredient or API, and any other bits and pieces called excipients that bind it together and make it look and taste better, may be crushed and an XRD pattern obtained from the powder to make sure that the API is in the form that is desired by looking for "fingerprints" of the correct and incorrect forms of the drug. As shown in Fig. 11.1, this all works rather well, until the API is present in an amorphous or nanocrystalline form, in which case the Bragg peaks, and the fingerprint, disappear. The amorphous XRD pattern is broad and featureless and not suitable for fingerprinting.

A question that has been addressed recently is whether PDF can help to fingerprint amorphous and nanocrystalline drugs (Bates *et al*., 2006; Billinge *et al*., 2010). Furthermore, if PDF can yield more information about the nature

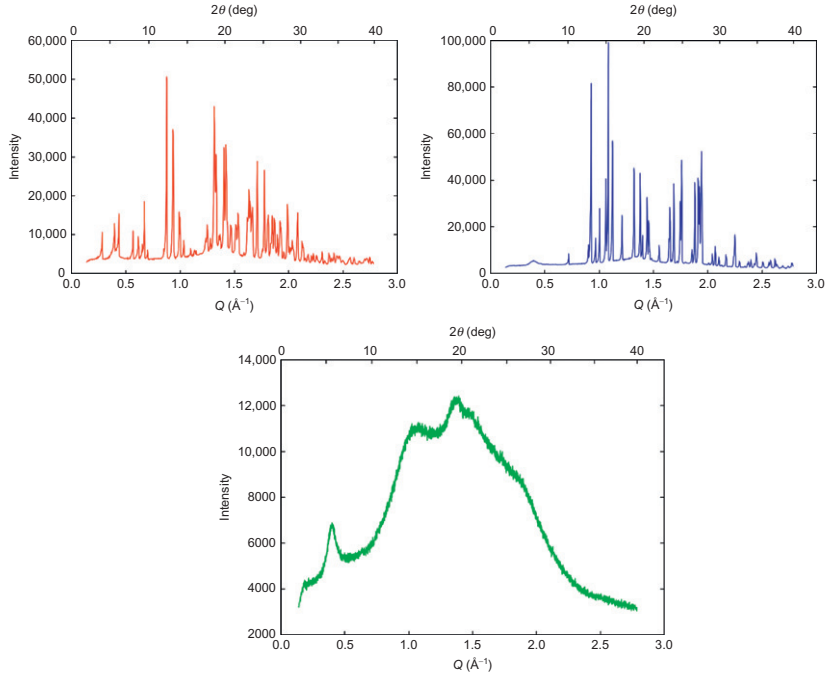

FIGURE 11.1 XRD fingerprints of different polymorphs of pharmaceutical carbamazepine (CBZ). Data are collected with a copper K_α laboratory diffractometer measured to a maximum angle of $2\theta = 40°$ following standard practice. Top left is the stable γ-crystalline form, top right is another crystalline polymorph called β. Below is the equivalent XRD pattern from a melt-quenched sample of CBZ that is "X-ray amorphous."

of local molecular packing in molecular systems exposed to different processing conditions, it can become an important tool in drug development. This is a growing need. Many of the drugs under consideration for next-generation therapies are much less soluble than in the past. The trend is toward finding drug targets that are larger and more flexible molecules. These often pack better in the solid state with strong hydrogen bonding and can be quite insoluble, sometimes referred to in the pharmaceutical industry as "brick dust" (Wassvik *et al*., 2008). The molecule may have a powerful pharmacological action, but how to get it into the patient's blood stream? The amorphous and nanocrystalline states present an opportunity because the solubility of these phases is much higher, as much as 20–100 times more soluble than the crystalline phases, so there is currently great interest in the amorphous phase of pharmaceuticals, but few precise experimental probes of it.

A possible role for PDF was first suggested in the early part of this millennium (Sheth *et al*., 2005; Bates *et al*., 2006), where the proposal was simply to transform into real space the copper K_α XRD patterns normally used for fingerprinting, such as those shown in Fig. 11.1. This approach is of limited value from the point of view that the Fourier transform does not add (or take

away) any information. So, as shown in Fig. 11.2, although the PDF appears to have more peaks in it than the original data, actually it does not contain any more information. The peaks in the PDF are ripples of the damped sine waves of the (roughly) two Fourier components corresponding to the two unresolved peaks in the original data. Thus, if there is insufficient information in the original data to fingerprint the material, there will be insufficient information in the PDF. Despite these difficulties, a number of follow-up studies (Bates *et al*., 2007; Heinz *et al*., 2008; Moore *et al*., 2009, 2010; Nollenberger *et al*., 2009; Engers *et al*., 2010; Botker *et al*., 2011; Padilla *et al*., 2011) have

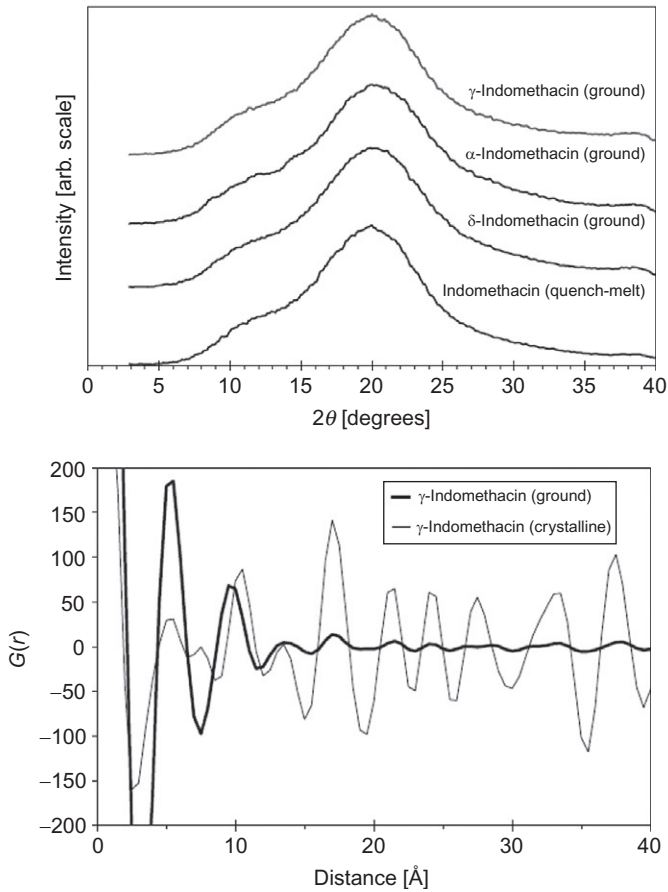

FIGURE 11.2 Left: XRD patterns from "X-ray amorphous" cryo-milled or quenched pharmaceutical indomethacin samples. Roughly two unresolved peaks are evident (right). The thick solid line shows a PDF function obtained from the top curve in the left panel, with many peaks evident. The pale curve is the PDF from γ-form crystalline indomethacin from data collected over the same range. There appear to be many more peaks in the amorphous PDF than in the original data. However, the information content is the same. Reproduced with permission (Bates *et al*., 2006).

applied this methodology to study various topics of interest in amorphous and nanocrystalline pharmaceuticals, which is a measure of the interest and the need in this area. It is clearly of the greatest interest to see what kind of information can be obtained from a total-scattering PDF type of experiment, along the lines described in this book, on amorphous pharmaceuticals. The results look very encouraging, as described below.

To differentiate the high-Q experiments, we describe here from the earlier low-Q experiments exemplified by the approach of Bates *et al.* (2006); we refer to them as total-scattering PDF or TSPDF measurements (Billinge *et al.*, 2010). The earlier PDF experiments were measured over an angular range of around $2\theta = 40°$ using copper K_α X-rays ($\lambda = 1.54$ Å) giving a Q_{max} of 2.8 $Å^{-1}$. The TSPDF measurements yielded usable data to up to $Q_{max} \sim 20$ $Å^{-1}$, more than seven times the range of data of the low-Q PDFs. The rapid acquisition PDF geometry was used and initial data collected at beamline ID11B at the Advanced Photon Source. The crystalline polymorphs and a sample of melt-quenched γ-form carbamazepine (CBZ) were measured. Indomethacin was also studied though the results are not reported here. The resulting $F(Q)$ and $G(r)$ functions are shown in Fig. 11.3. There is clearly a great deal more structural information in these data than the low-Q data. The low-r regions of all three PDFs are very similar, reflecting the fact that the PDFs are all from the same molecule. In the high-r region, above around 3 Å, there are ripples that appear rather small, especially in

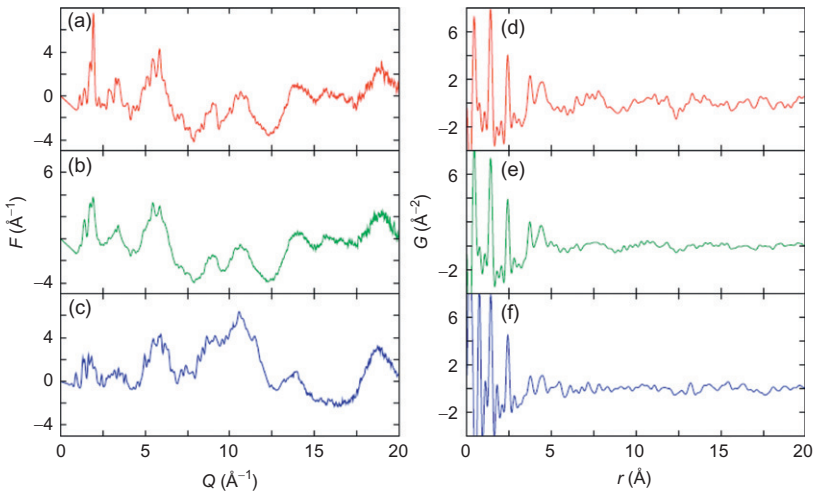

FIGURE 11.3 Left: Total scattering reduced structure functions, $F(Q)$, from three samples of carbamazepine. (a) β-crystalline form, (b) melt-quenched, and (c) γ-crystalline form. The data were collected using high-energy synchrotron X-rays. Right: The resulting PDFs obtained by Fourier transforming the data in the left panel (Billinge *et al.*, 2010).

the melt-quenched sample, but do show some similarities between the middle and the top panels. We can emphasize the features in this high-r region of the PDF by plotting the data on an expanded y-scale, choosing to plot the PDF of the melt-quenched sample on top of that of the β-crystalline form, in Fig. 11.4. The two curves are clearly highly similar. It is not shown here, but the same similarity is not seen with respect to the γ-crystalline form whose PDF is quite different. This clearly establishes that the packing in the melt-quenched sample is locally like that in the β-crystalline form, even though it was the γ-form of the drug that was originally melted. We can go further than this. We see in the figure that the amplitude of the PDF features of the melt-quenched sample diminishes with increasing r due to the noncrystalline short-range order in the material. If for simplicity we assume that the domain of local order is spherical, we can use the method described in Chapter 6 and make a correction to the PDF to account for this nanocrystallinity by dividing by the particle form factor. When we do this, there is a single parameter which is the diameter of the nanocrystalline domain. In the right panel of Fig. 11.4, the PDF of the melt-quenched sample, corrected for a nanocrystalline domain size of 4.5 nm, is shown plotted on top of the β-crystalline form PDF. The similarity is now striking. The melt-quenched sample clearly consists of 4.5-nm diameter domains of local nanocrystalline order with β-form packing.

The wealth of detail evident in Fig. 11.4 shows that, at least in cases where there is nanoscale range local packing of molecules, the TSPDF approach clearly presents enough information for fingerprinting even when there is no long-range crystalline order in the material.

As well as making a visual inspection of the plots in Fig. 11.4, it is helpful to have a more quantitative measure of their "similarity" to help automate any

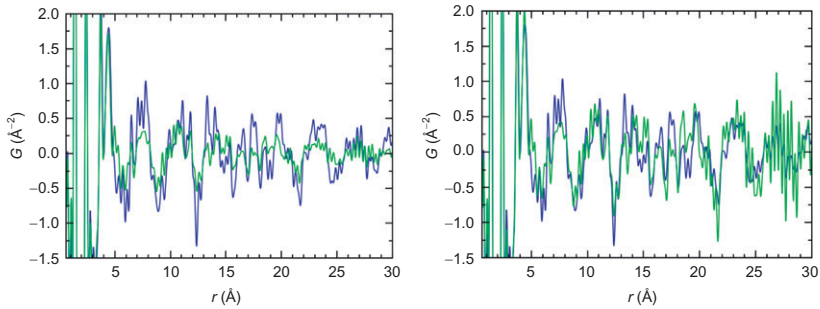

FIGURE 11.4 Left: PDFs of the β-crystalline form of CBZ (larger amplitude ripples) and the melt-quenched sample, plotted on a y-scale to emphasize the ripples in the high-r region. The two curves reproduce each other rather well. Right: The same two curves as shown in the left panel, however, with the melt-quenched sample being corrected for size effects assuming it is a 4.5-nm diameter spherical nanostructure.

fingerprinting process. What is used in modeling is a weighted profile agreement factor, f_w (see Chapter 6), which is the integration (or more accurately the sum) of the square of the difference between the calculated and measured PDFs over the range of fitting of the data. Each point is weighted by the square of the statistical uncertainty of the data on that point. Something similar can be used here where the calculated model PDF may be replaced with a measured PDF from the calibration sample. For example, the reference data set may be a measured PDF from the crystalline β-form of the material that is being compared with the PDF from the melt-quenched sample. In this case, the reference PDF should be processed with the same Q_{max} as the sample under test. A slight problem with this approach is that a large f_w may be obtained for reasons other than the similarity of the signal, for example, if the scale factors of the reference and test PDFs are different. This could be corrected by rescaling. However, an alternative approach that removes this scale-factor effect is to calculate a different, scale independent, measure of sameness, for example, the Pearson product–momentum correlation (Myers *et al.*, 2010), which is given by

$$r_p = \frac{1}{1-n}\sum_{i=0}^{n}\left(\frac{X_i-\bar{X}}{\sigma_X}\right)\left(\frac{Y_i-\bar{Y}}{\sigma_Y}\right). \tag{11.1}$$

In this context, X and Y refer to the two PDFs being compared and the sum is over all the points in the PDFs within the range being compared, and $\bar{X}$ and σ_X are the mean and standard deviation of those two functions, given by $\bar{X} = \frac{1}{n+1}\sum_{i=0}^{n} X_i$ and $\sigma_{X^2} = \frac{1}{n+1}\sum_{i=0}^{n}(X_i-\bar{X})^2$, as discussed in more detail in Dykhne *et al.* (2011). This function, and others like it such as the Spearman correlation factor used in the commercial software PolySnap (Barr *et al.*, 2004), take the value 1 when the two curves are the same (i.e., perfectly correlated), -1 when they are opposite to each other (i.e., perfectly anticorrelated), and zero when the two curves are uncorrelated. This approach works very well (Dykhne *et al.*, 2011) in practice. It is found that the PDFs from many different molecular compounds tend to be weakly correlated (i.e., it is usual to obtain positive numbers for r_p when comparing many different PDF curves from molecular systems), presumably because of universal characteristics of the PDF function itself and commonalities in the samples. However, TSPDFs from samples with similar underlying structures have high correlation factors, and a rule of thumb has emerged that correlations exceeding 0.8 probably signify the presence of the same packing and warrant a deeper study. All molecular materials have similar PDFs in the very low-r region (they all share similar C—H and C—C bonds), and different polymorphs of the same molecule share even more features coming from the intramolecular PDF. When the main interest is to study nanopolymorphism, that is, molecular packing on the nanoscale, rather than the structure of the molecule itself, the correlation functions have greater sensitivity

if a range of r is chosen to calculate the correlation function that does not include the near neighbor peak and a value or r_{min} of 3 Å is often chosen in r_p (Eq. 11.1). In the future, this use of correlation functions for assessing similarity of API nanostructures should become more powerful as more accurate protocols using this approach are developed.

11.3. SENSITIVITY DEPENDENCE ON Q_{MAX}

It is evident from the $F(Q)$ functions in Fig. 11.3 that a significant amount of information is contained in the scattering beyond $Q \sim 3$ Å^{-1} where the original PDF studies (Bates *et al*., 2006) terminated their measurement and that there is a clear benefit to measuring data over a wider Q-range. Even though the domain size, d, is of the order of nm, we cannot terminate the Q-range of measurement at $2\pi/d$. The information obtained by the signal around $2\pi/d$ is merely the *size* of the domain, and the information about the *nature* of the domain is contained in the Q-range way beyond $2\pi/d$. It is interesting to know in greater detail how this variation in information content affects fingerprinting. This has been studied in some detail (Dykhne *et al*., 2011). In this study, high Q_{max} TSPDF data measured at a synchrotron source were systematically degraded by transforming at lower and lower Q_{max} values that would simulate different situations that one might encounter in the lab, that is, collecting data over some range using a laboratory X-ray source with not only as the ubiquitous copper but also molybdenum and silver sources. The results are shown in Fig. 11.5. The left panel shows data from the melt-quenched CBZ, which we know consists of 4.5-nm diameter nanodomains of β-form packing. The right panel shows the PDF from β-crystalline material. Comparing the left and right panels, the similarities are apparent, as already noted above. Comparing the curves from the top to the bottom, the effect of decreasing Q_{max} is immediately apparent as a loss in resolution of the measurement. In the intermediate-r range of interest for studies of molecular packing, it appears that nearly all of the relevant information survives down to a Q_{max} of 12.5 Å, readily achievable from a Mo source. However, there is significant loss of information in this range for lower Q_{max} values available from copper sources.

What about the sensitivity for fingerprinting? The demonstration of the similarity between PDFs, albeit with lower resolution, of limiting Q_{max} is only half the story when it comes to fingerprinting. The other half of the story is the ability of the data to differentiate PDFs from samples with a different packing. To fingerprint, you need positive correlations when two PDFs are alike, but you must not have false positives from unlike samples. This was tested systematically with these data. The finding was that the Pearson correlation coefficients remained high when comparing the melt-quenched PDFs with the crystalline β-form for all Q_{max} values, but as the *information content in the data decreased*, all of *the correlation coefficients increased* resulting in false positives for data below $Q_{max} = 12.5$ Å. For the higher Q_{max} data, the correlation analysis showed

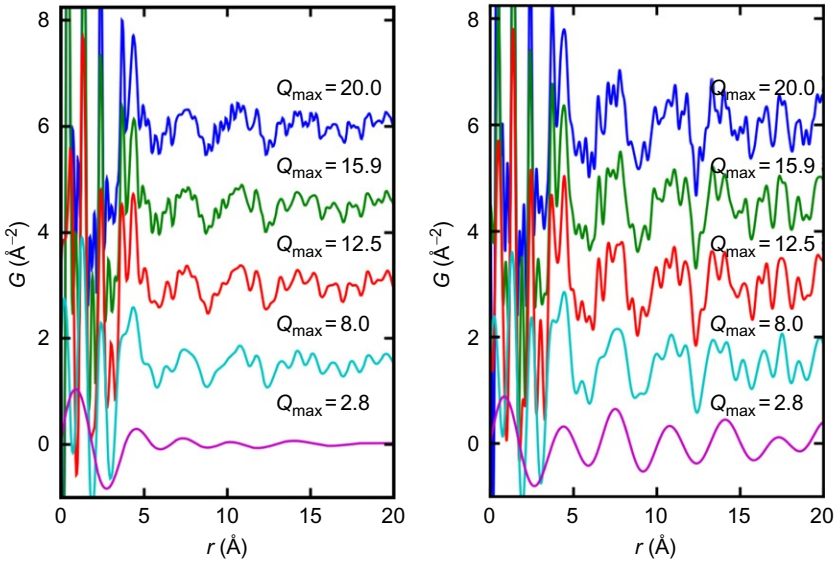

FIGURE 11.5 PDFs of CBZ obtained from the same data sets but with the raw data cut at different values of Q_{max} before processing. Left: PDFs from melt-quenched CBZ. Right: PDFs from β-form crystalline CBZ. As Q_{max} is reduced, the resolution and information content of the measurement is systematically reduced. The values of Q_{max} chosen roughly correspond to the range of data it is possible to obtain from (from top to bottom) a silver laboratory X-ray source, a Molybdenum source, a Mo source collecting data to $2\theta = 90°$, a copper source, and a copper source measured to $2\theta = 40°$ (Dykhne *et al.*, 2011).

a significant correlation between the melt-quenched test sample and the crystalline β-form reference sample, but no significant correlations with other reference samples. Beginning with the $Q_{max} = 8$ Å data set, significant correlations were found between the PDF of the melt-quenched sample and with both the β- and γ-crystalline forms of CBZ. For the $Q_{max} = 2.8$ Å data set, the results were all over the place. In this case, significant correlations were found between melt-quenched CBZ and an α-crystalline form of indomethacin (a completely different molecule) and an amorphous form of indomethacin, and somewhat surprisingly, there was no significant correlation between the melt-quenched CBZ and its crystalline β-form, which is actually the correct answer. This may be due to the difficulty of obtaining a correct transform to the PDF when the asymptotic behavior or the $S(Q)$ is not clearly established by measuring it over sufficiently wide a Q-range (Dykhne *et al.*, 2011). Fingerprinting with such a low Q_{max} is clearly highly unreliable.

As an addendum to the discussion on information content in the data, it is possible to use information theory to place limits on what can be learned from the PDF given by a particular data set by plotting the PDF on a grid which has the Nyquist–Shannon sampling frequency (Shannon, 1949), as discussed in

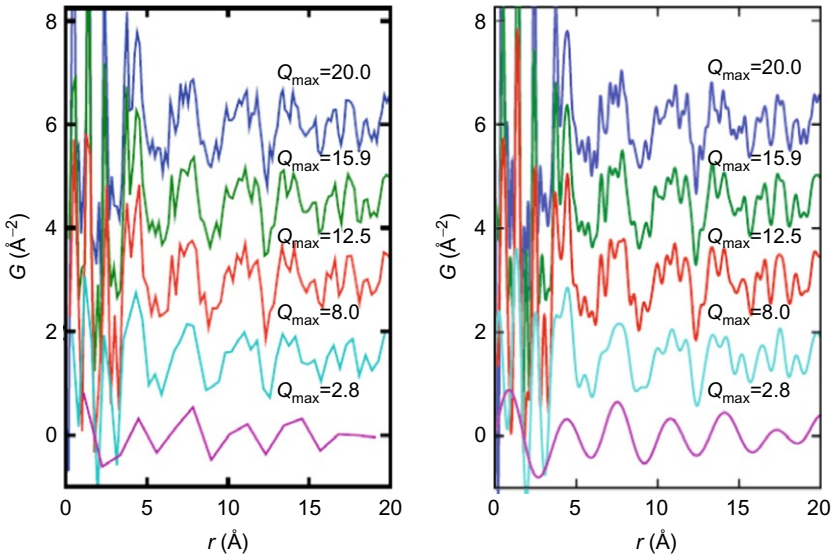

FIGURE 11.6 PDFs from β-form crystalline CBZ obtained from the same data set terminated at different values of Q_{max}. Left: The PDFs are plotted on the Nyquist–Shannon sampling grid appropriate for the particular value of Q_{max} chosen. Right: The PDFs plotted on the same fine grid as each other of 0.01 Å. These are the same PDFs shown in the right panel of Fig. 11.5, reproduced here for ease of comparison. The lowest Q_{max} data consist of around 15 points (Dykhne *et al.*, 2011).

Chapters 5 and 6. The current data are shown in Fig. 11.6 (left panel) plotted on the Nyquist grid. For convenience, in the right panel, we reproduce the data from Fig. 11.5 that were plotted on a finer grid. The theory states, and it has been demonstrated practically (Farrow *et al.*, 2011), that the data plotted on this grid contain the same information as when it is plotted on a finer grid. In other words, the PDFs shown in the left and right panels of Fig. 11.6 are absolutely equivalent. The loss in information on reducing Q_{max} is graphically illustrated, with the lowest Q_{max} data having only around 15 points over a range of 20 inverse angstroms.

For the high Q_{max} TSPDF measurements, it is clear that they can contain a great deal of information and we are confident that this method will be very useful in the study of amorphous and nanocrystalline drugs in the future. As well as simply fingerprinting compounds, one can think of many additional applications for the method. Time-dependent TSPDF studies could be carried out to assess stability of amorphous and nanocrystalline drug products. TSPDF experiments on samples that contain mixtures of crystalline and amorphous material may be studied to quantify the amount of amorphous material in the mixture. Indeed, phase quantifications could be carried out on more complex mixtures of crystalline and amorphous materials. Spatially resolved

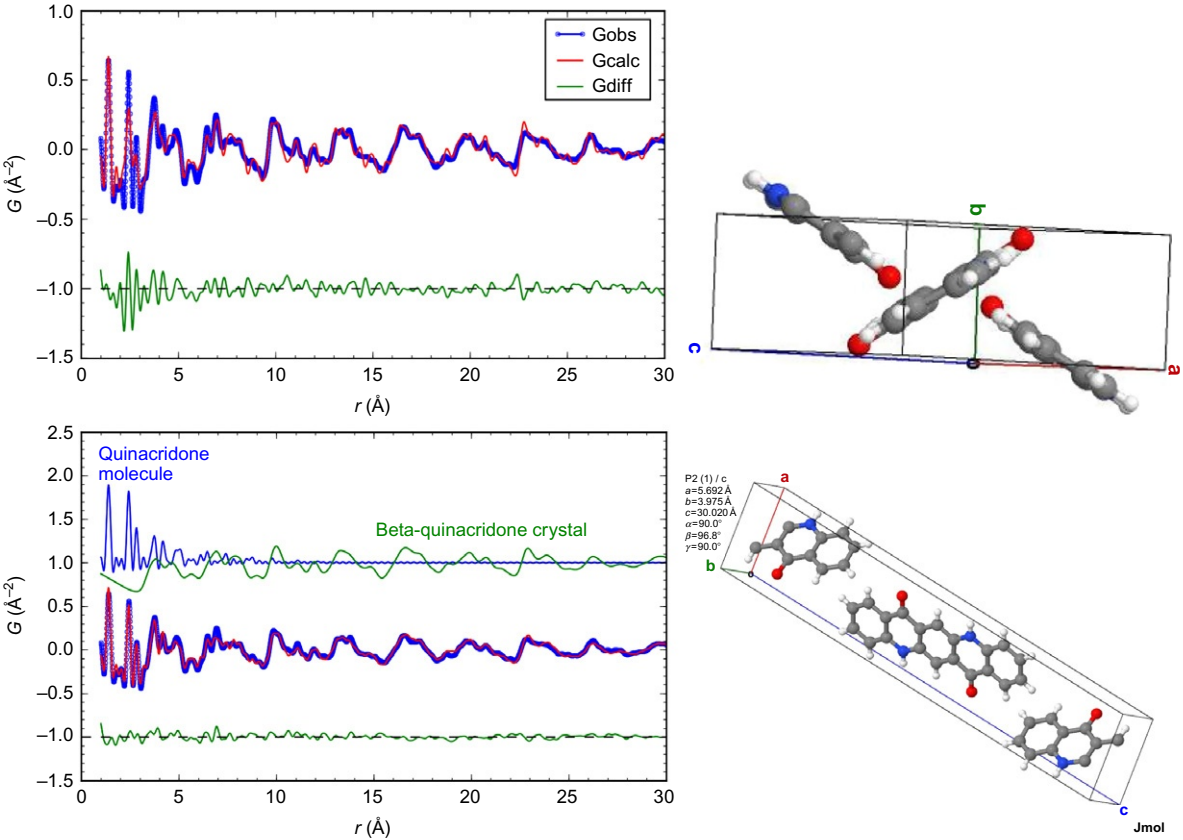

FIGURE 11.7 Model fits of molecular systems to TSPDFs. The data are from β-form crystalline quinacridone which is a commercial red/purple pigment. The molecule and the packing are shown from two different aspects on the right. Top left: The best fit of a crystalline model. The open circles are the data and the solid line is the fit. Offset below is a difference curve. The peaks are in the right place, but at high-r the model peaks are too sharp compared to the data and at low-r the model peaks are too broad. The fit has made a compromise by assigning ADPs that are intermediate between the ADPs appropriate for intramolecular (sharp peaks) and intermolecular (broad peaks) PDFs. Lower left: To correct for this the new program, SrFit, has been used to separately fit the inter- and intramolecular PDFs. The fit is now satisfactory.

measurements, for example, as a function of position on a pill, could be carried out to assess the uniformity of the pill and to quantify the distribution of different products through the pill. Samples could be studied as a function of different processing parameters to assess things such as nanocrystalline packing and nanocrystalline particle size as a function of different processing steps or different formulations of a product. At the time of writing, such studies are already underway to benchmark the method and develop protocols for doing these different tasks and we expect rapid progress in the coming years. There will be similar applications in other areas where small molecules are important, such as pigments and molecular electronics.

11.4. MODELING MOLECULAR SYSTEMS

Finally, data that are rich in structural information may be modeled in a similar way as is done for inorganic materials to obtain more precise information. Given a known crystal structure, the PDF can be readily calculated and we have done this using PDFgui (Farrow *et al*., 2007) with good results. However, special software is needed for refining crystal structures of molecules where the objective is to move atoms around collectively without changing the molecule except in allowed ways that activate internal degrees of freedom such as freely rotating bonds. The SrFit modeling software that is under development will have this capability and fits where bond-length and bond-angle constraints have been respected has already been tested. A special challenge for PDF studies, which is not relevant for crystallographic studies, is that there is significant correlated motion in molecular systems (see Chapter 7). This means that PDF peaks from mutually rigid parts of a molecule, such as near neighbor bonds or rigid rings, are very sharp in the PDF whereas intermolecular correlations tend to be broad. Software needs to be developed to handle this case properly, although a simple workaround has shown itself to be effective using the SrFit software as shown in Fig. 11.7. This consists of making a three-phase fit to the data consisting of the crystal structure to fit the intermolecular PDF peaks coming from the packing. These peaks are broad and this model results in low-r intramolecular peaks that are much too broad. A feature of the SrFit program is that it can calculate PDFs from single molecules and clusters. The two other PDFs that are added to the fit to the data are both from the molecule itself. The first uses the same atomic displacement factors (ADPs) as were obtained from the crystallographic model and a negative scale factor so that the broad intramolecular peaks are subtracted from the fit. Finally, the PDF of the same molecular structure is calculated with a positive scale factor and ADPs that give the sharp peaks seen in the data.

REFERENCES

Barr, G., Dong, W. & Gilmore, C.J. (2004) *J. Appl. Crystallogr.*, **37**, 658–664.

Bates, S., Zografi, G., Engers, D., Morris, K., Crowley, K. & Newman, A. (2006) *Pharm. Res.*, **23**, 2333–2349.

Bates, S., Kelly, R.C., Ivanisevic, I., Schields, P., Zografi, G. & Newman, A.W. (2007) *J. Pharm. Sci*., **96**, 1418–1433.

Belyakov, A.V., Baskakov, A.A., Berger, R.J.F., Mitzel, N.W., Oberhammer, H., Arnason, I. & Wallevik, S.O. (2012) *J. Mol. Struct*., **1012**, 126–130.

Bernstein, J. (2002) *Polymorphism in Molecular Crystals*. Oxford: OUP.

Billinge, S.J.L., Dykhne, T., Juhas, P., Bozin, E.S., Taylor, R., Florence, A.J. & Shankland, K. (2010) *CrystEngComm*, **12**, 1366–1368.

Botker, J.P., Karmwar, P., Strachan, C.J., Cornett, C., Tian, F., Zujovic, Z., Rantanen, J. & Rades, T. (2011) *Int. J. Pharm*., **417**, 112–119.

Dykhne, T., Taylor, R., Florence, A. & Billinge, S.J.L. (2011) *Pharm. Res*., **28**, 1041–1048.

Engers, D., Teng, J., Jimenez-Novoa, J., Gent, P., Hossack, S., Campbell, C., Thomson, J., Ivanisevic, I., Templeton, A., Byrn, S. & Newman, A. (2010) *J. Pharm. Sci*., **99**, 3901–3922.

Farrow, C.L., Juhas, P., Liu, J.W., Bryndin, D., Bozin, E.S., Bloch, J., Proffen, T. & Billinge, S.J.L. (2007) *J. Phys. Condens. Matter*, **19**, 335219.

Farrow, C.L., Shaw, M., Kim, H., Juhas, P. & Billinge, S.J.L. (2011) *Phys. Rev. B*, **84**, 134105.

Hancock, B.C. & Parks, M. (2000) *Pharm. Res*., **17**, 397–404.

Hancock, B.C. & Zograf, G. (1997) *J. Pharm. Sci*., **86**, 1–12.

Heinz, A., Strachan, C.J., Atassi, F., Gordon, K.C. & Rades, T. (2008) *Cryst. Growth Des*., **8**(1), 119–127.

Kline, R.J., McGehee, M.D. & Toney, M.F. (2006) *Nat. Mater*., **5**, 222–228.

Mark, H. & Weirl, R. (1930) *Naturwissenschaften*, **18**, 205.

Moore, M.D., Steinbach, A.M., Buckner, I.S. & Wildfong, P.L.D. (2009) *Pharm. Res*., **26**, 2429–2437.

Moore, M.D., Shi, Z. & Wildfong, P.L.D. (2010) *Pharm. Res*., **27**, 2624–2632.

Myers, J.L., Well, A.D. & Lorch, R.F. (2010) *Research Design and Statistical Analysis* (3rd Edition). New York: Routledge Academic.

Nollenberger, K., Gryczke, A., Meier, C., Dressman, J., Schmidt, M.U. & Bruehne, S. (2009) *J. Pharm. Sci*., **98**, 1476–1486.

Padilla, A.M., Ivanisevic, I., Yang, Y., Engers, D., Bogner, R.H. & Pikal, M.J. (2011) *J. Pharm. Sci*., **100**, 206–222.

Paulus, E.F., Leusen, F.J.J. & Schmidt, M.U. (2007) *CrystEngComm*, **9**, 131–143.

Shainyan, B.A., Kirpichenko, S.V., Shlykov, S.A. & Keinpeter, E. (2012) *J. Phys. Chem. A*, **116**, 784–789.

Shannon, C.E. (1949) *Proc. IRE*, **37**, 10–21.

Sheth, A.R., Bates, S., Muller, F.X. & Grant, D.J.W. (2005) *Cryst. Growth Des*., **5**, 571–578.

Spirk, S., Berger, R.J.F., Reuter, C.G., Pietschnig, R. & Mitzel, N.W. (2012) *Dalton Trans*., **41**, 3630–3632.

Wassvik, C.M., Holmen, A.G., Draheim, R., Artursson, P. & Bergstrom, C.A.S. (2008) *J. Med. Chem*., **51**, 3035–3039.

Zewail, A.H. (2006) *Annu. Rev. Phys. Chem*., **57**, 65–103.